Computer Aided Detection Method for Ischemic Stroke Using Feature Based Approach

Y LI[1], DKS NG[2], JMY KWOK[3]

[1]Department of Mathematics, The City University of Hong Kong, Hong Kong
Email: yanli66-c@my.cityu.edu.hk
[2]School of Science and Technology, The Open University of Hong Kong, Hong Kong
Email: dng@ouhk.edu.hk
[3]Faculty of Health and Social Sciences, The Hong Kong Polytechnic University, Hong Kong
Email: manyee.kwok@connect.polyu.hk

Abstract— *In this paper we have proposed a Computer Aided Detection (CAD) scheme for the early detection of Ischemic Stroke using Adaptive Region of interest. A number of statistical parameters such as Energy and Entropy will be calculated from the Adaptive Region of interest and these will be compared with the contra-lateral side of the brain.*

Keywords— Ischemic stroke, Computer aided detection, Adaptive region of interest, image features.

I. INTRODUCTION

The human brain is the most complex and metabollically demanding organ of the entire body. It is a jelly-like mass of tissue comprising about 2.5% of the total body weight [1]. It takes about 20% of the body's oxygen consumption. The brain consists of forebrain, midbrain and hindbrain. It controls the central nervous system (CNS) via the cranial nerves and spinal cord. It also controls the peripheral nervous system (PNS) and regulates virtually all human activities. We can control our mental activity consciously such as thought, action, memory, feeling and experience of the world. A disturbance to the cerebral blood vessels or cerebral blood flow will lead to disastrous consequences. The vascular disease of the brain is called cerebrovascular accident (CVA) or stroke.

With the aging of our population, stroke has been rated the third highest cause of death (second to heart disease and cancer) in the world. In the USA, it was estimated that there were about 700,000 new and recurrent cases of stroke per year [2]. In Hong Kong, there were around 16,000 new/recurrent cases of stroke and more than 3,000 people died due to stroke per year [3]. Stroke results from insufficient supply of oxygen and nutrient to the brain tissues. The nerve cells die, and there is no replacement of nerve cells. Therefore, the nervous system will deteriorate and this will affect the normal functions of the body. As a result, the loss of function appears rapidly even within minutes. The major types of stroke are ischemic stroke and hemorrhagic stroke. The symptoms of stroke include acute hemi-paresis, aphasia, non-focal neurological deflect, etc. Most cases involve ischemic stroke rather than hemorrhagic stroke in the ratio of 80% versus 20%. In addition, ischemic stroke is more common in the Chinese community (Ho, 2002). Among these patients, only about 10% could fully recover. Therefore, this has been a leading cause of severe and long-term disability with huge direct and indirect cost to society [2].

Diagnosis of the type of stroke must be accurate. In the emergency department, 20% of the diagnosis might be incorrect [4]. In addition to the neurological examination, if the Glasgow Coma Scale (GCS) [5] or National Institutes of Health Stroke Scale (NIHSS) [6] lies somewhere between severe and moderate level, patients are required to undergo an emergency brain scan, for example, Computed Tomography (CT) or Magnetic Resonance Imaging (MRI). Other imaging modalities such as Positron Emission Tomography (PET) and Single Photon Emission Computed Tomography (SPECT) are available for diagnosis of brain diseases.

CT is significantly more sensitive to gradations of tissue density than a conventional X-ray. Each pixel in the CT image is assigned a numerical value called CT number (in Hounsfield Units, HU). The image will appear to be white if the CT number is large or vice versa. For example, the bony structure has CT number ranging from 80 to 1000, which appears in white in the CT image. A gradual decline of the CT number by 0.4 HU every hour was reported during the first 6 hours after the onset of acute ischemic stroke [7]. The mean reduction of CT number was reported to be 1.3 HU at 2.5 hours after the onset. These studies indicated that differences 2-4 HU needed to be recognized to detect early CT signs of ischemic brain damage during the early hours after the onset of ischemic stroke [8]. With CT images, the most contrast occurs among bone, brain tissue, and cerebrospinal fluid (CSF). Bone appears bright, CSF appears dark, and brain tissue appears somewhat in between. Modern CT scanners produce fine-grained resolution, permitting some differentiation between white and gray

matter. Unfortunately, even with high-resolution scanners, a CT image is almost always less precise than it appears. With an MRI scan it is possible to take images from different sections at almost every angle, whereas a CT scan only shows cross-sectional images. There is no ionizing radiation (X-rays) involved in producing an MRI scan. MRI scans are generally for imaging soft tissue. Therefore, it gives more detailed, too. The difference between normal and abnormal tissue is often clearer on the MRI scan than on the CT scan. This is due to the fact that MRI can more easily differentiate tissues than CT, not due to resolution, but for bone, CT is better.

However, CT remains the choice for the evaluation of patients with suspected acute ischemic stroke due to the following reasons: compared to MRI, brain imaging with CT is more accessible in clinical setting, less expensive to operate, quicker in scanning time and more reliable [9]. Some patients cannot undergo MRI because of claustrophobia. MRI is also not feasible if patients have metallic implant, like metallic heart valves, aneurysm clips or other ferromagnetic material which will be affected by the strong magnetic field. Moreover, patients with severe bleeding are not suitable for MRI scanning, because the blood clots will become a tissue which is difficult to distinguish from the normal tissue. As a result, CT remains the first line of imaging in the clinical setting [10].

For severely ill patients, CT scanning is able to rule out cerebral hemorrhage or early signs of major cerebral infarction - both symptoms are contra-indications to thrombolytic therapy. If necessary, a follow up MRI scan could be used as a screening process for thrombolytic therapy. Large diffusion signal abnormality in MRI indicates significant brain cell death and so a poor candidate for thrombolytic therapy; whereas predominant perfusion abnormality in MRI indicates salvageable brain tissues and good indication for thrombolytic therapy [11].

Early CT scan findings in ischemic stroke can be evident within 2-6 hours and these include effacement of sulci, loss of normal gray-white junction, loss of the insular ribbon, mass effect and dense MCA sign [12]. Therefore, a proper treatment consideration must be assigned promptly and correctly according to the CT images.

In most parts of the world, acute care physicians, emergency physicians, internists, neurosurgeons are the ones who read the CT images at odd hours, when radiologist's expertise may not be immediately available [13]. This requires huge logistics demands, costs, manpower and scanning facilities. This solely relies on the availability of manpower in the hospital. Therefore, the chance of misdiagnosis will depend on the performance of observers. The interpretation skills of brain CT by acute care physicians have been shown to be imperfect [14].

The variation of the performance of interobservers will greatly affect the patient care and there is a need to enhance the performance of observers, especially for non-radiologists. Therefore, early detection of stroke is important and we propose a Computer-Aided Detection (CAD) method to minimize the false positive rate.

The concept of CAD is based on the assumption or expectation that machines and computers are better in certain tasks than humans, and thus abnormalities would be detected by use of a computer, which enhances radiologists' detection capabilities. The effect of computer output on radiologists' image interpretation is usually not taken into account. Therefore, research efforts on automated diagnoses were focused only on the development of computer algorithms

The goal of CAD is to improve the quality and the productivity of clinicians' tasks by improving the accuracy and consistency in radiological diagnoses and also by reducing the image reading time (reducing the sectional images of the brain scan). The general approach for CAD is to find the location of a lesion, and also to determine an estimate of the probability of a disease; these correspond to CAD for the detection of the lesion and CAD for differential diagnosis.

Nowadays, CAD has many applications in the field of medical imaging, such as the diagnosis of breast cancer [15][16][17] and lung cancer [18] [19].

II. MATERIALS AND METHODS

2.1 Materials

A total of 88 cases from 62 different subjects of Computed Tomography (CT) scan were collected from our collaborative hospital between 2014 and 2015. We excluded some cases due to the poor image quality and the fact that the neuro-radiologists did not agree with the diagnostic report. The remaining cases include 30 subjects showing ischemic changes (18 acute subjects and 12 chronic subjects) and 20 cases showing normal. The average age of the patients is 72.31 years old (ranging from 42-92 years old) with 28 males and 34 females. The image resolutions range from 0.35mm to 0.54mm per pixel. All the images were acquired from the single detector CT scanner manufactured by General Electric (GE) Medical

Systems. Each patient has around 18-24 axial images scanned parallel to the orbito-meatal line (OML) (Figure 1) according to the protocol by [20] and [21]. The slice thickness varies from 5mm to 10mm depending on the size of the skull. The images acquired were under the exposure of 140kVp and 200mA. Figure 2 shows a typical CT image set for a patient.

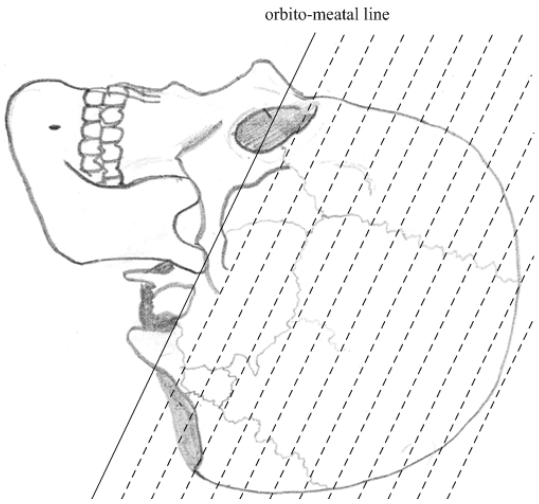

FIGURE 1: ORBITO-MEATAL LINE.

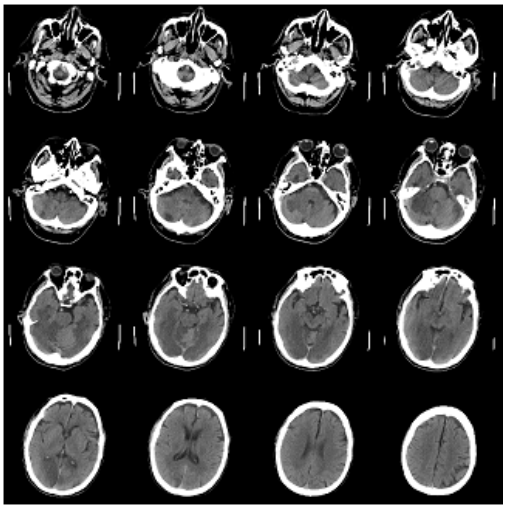

FIGURE 2: CT IMAGES SET FOR A PATIENT.

2.2 Radiological Diagnosis of Collected Cases

Table 1 shows the profile of the images collected from our collaborative hospital.

TABLE 1
DISTRIBUTION OF CASES.

Radiological diagnosis	No. of Cases	Training	Validation
Ischemic Stroke	30	5 acute cases 5 chronic cases	20
Control	20	10	10
Total	50	20	30

As the image features of chronic cases (which are very subtle to be seen by naked eye) and acute cases are different in CT, we have included the case of chronic ischemic stroke in the training data set to reduce the false positive rate. To increase the reliability of the program, the training data set will not be used again in the validation process.

2.3 CAD System

In regular radiological screening procedures, the occurrence of screening stroke is usually rare. True positive casess such as ischemic stroke are believed to occur at a rate of per hundred patient examinations. The use of a computer aided detection (CAD) system would serve as a reminder or second reader to help the radiologists to achieve a higher sensitivity. It was believed that the use of CAD in a clinical setting will continue to increase [22]. In later sections, several new algorithms were proposed to help to increase the detectability of stroke. The CAD system is developed using MATLAB (The Mathworks Inc., Release 2016a). The images are in Digital Imaging and Communication in Medicine (DICOM) format. All the patients' information was removed and images were loaded in the CAD program. The CAD program will assist to locate the region of stroke.

2.4 Interface of CAD

A new CAD system was proposed which would operate on CT medical images in DICOM format (*.dcm) or Windows bitmap format (*.bmp) with viewing resolution of the screen set to 1280×1024 square pixels. The input and output screens had dimension of 512×512 square pixels. To use the CAD system, users had to open the appropriate folder contains the images of the patient. The images would be displayed on the left screen of the CAD system, and then the users would be allowed to use to navigate the images forward and backward. The CAD system allowed the users to rate the certainty of

diagnosis using a 5 point Likert scale (1 = Definitely Absent, 2 = Absent, 3 = Uncertain, 4 = Present, 5 = Definitely Present) on each image. Afterward, the users had to activate the CAD program by pressing a CAD button, the CAD system would display the regions of having possibilities of abnormalities at the right hand side of the screen. Then, the users would be allowed to adjust their decisions according to the advice from the CAD system and save their decisions studies for future follow up. Figure 4.3 shows the layout of the CAD system.

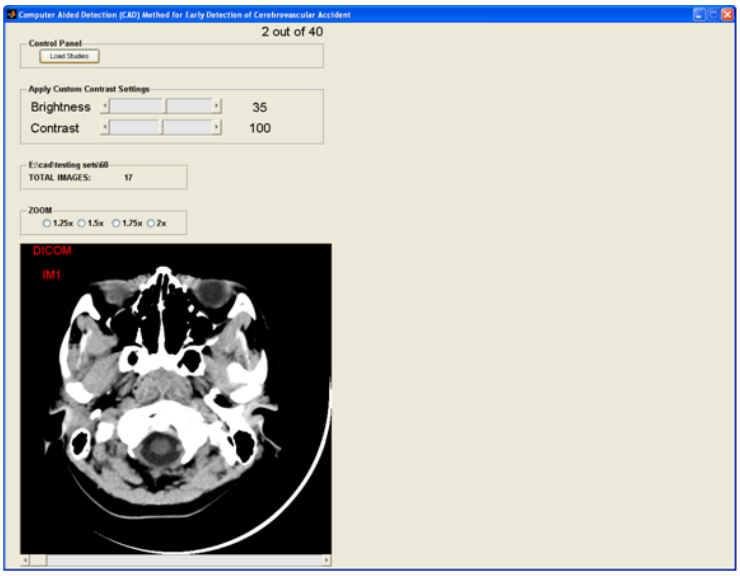

FIGURE 2.3: THE INTERFACE OF THE CAD SYSTEM.

The users had to click an open button to load the images of the appropriate patients in DICOM format and they would be allowed to adjust the window level and width such as brightness and contrast. They could also magnify the images by using an appropriate zooming factor (from 1.25, 1.5, 1.75, 2). For each patient, the users were required to comment (without CAD first and with CAD) on the stroke twice by choosing the appropriate scale. After all the scores were collected for all subjects, the real time receiver operating characteristics (ROC) curves would be generated to evaluate the performance of the readers on an individual basis.

2.5 Workflow of CAD

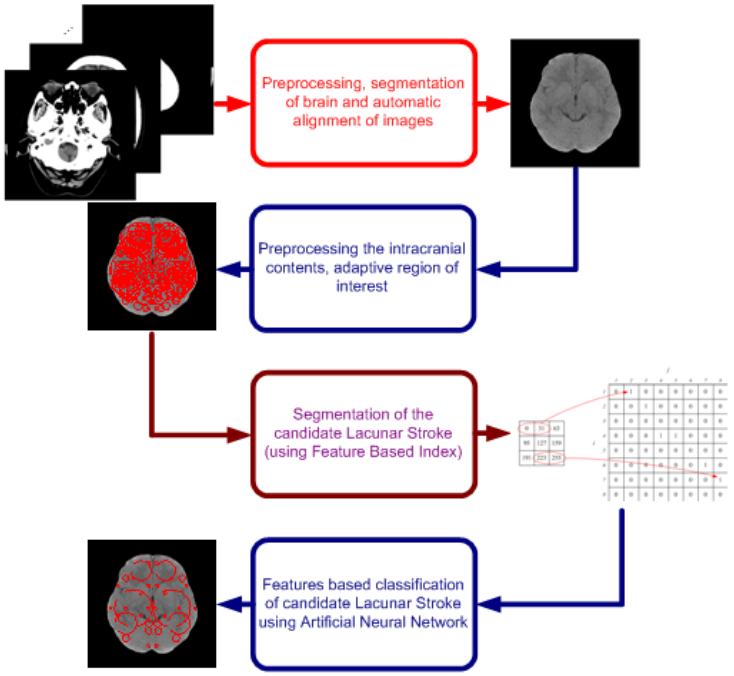

FIGURE 2.4: WORKFLOW OF CAD.

Algorithm 2.1 (*Rotation of sectional CT*):

1. Read the images in DICOM format
2. Find the best orientation of the sectional brain

The detailed implementation of Algorithm 2.1 will be discussed as follows:

First, we read in the DICOM images, which are stored in a 2D array for further processing; the DICOM header also contains the patient information, slice thickness and resolutions of the CT images, etc.

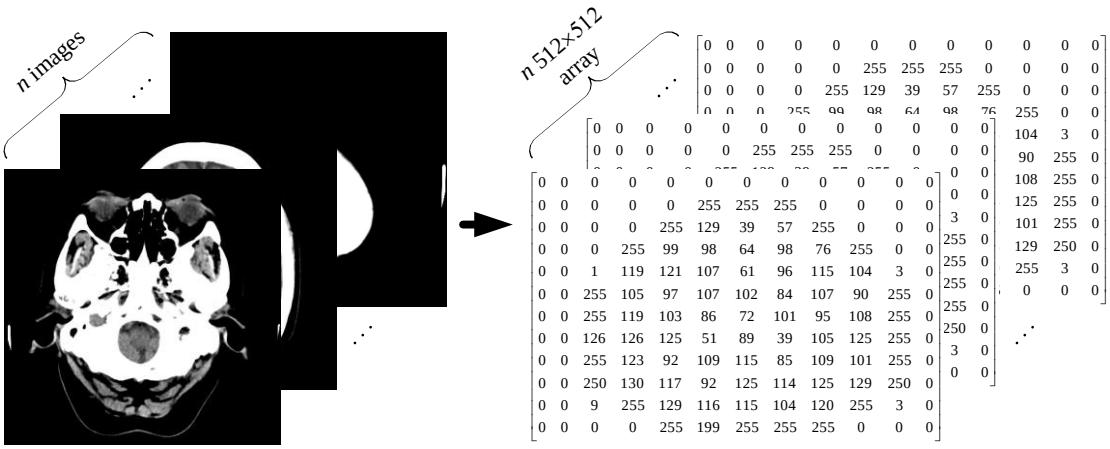

FIGURE 2.5: IMAGE REPRESENTATION OF CT.

In most of the urgent brain scan, the patients have lost consciousness. Therefore, the CT images obtained are not in their best orientation, and so we need to rotate the CT images of the brain according to some rules, which are based on the assumption that the human skull is symmetrical. We reconstruct the 3D volumetric images from the planar CT images, i.e., stack them up together according to the appropriate order of sectional level of the images.

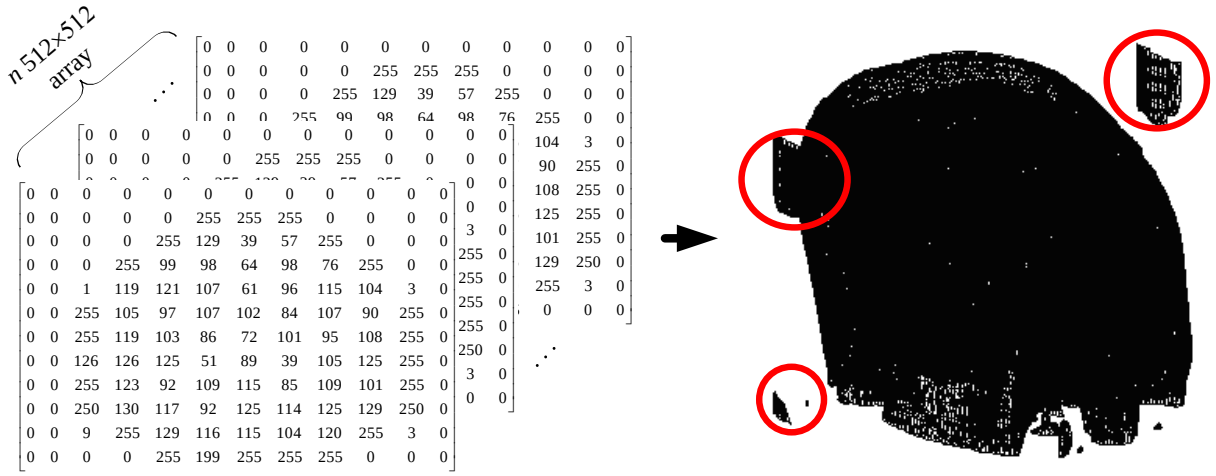

FIGURE 2.6: 3D RECONSTRUCTION OF CT.

We notice that some human artifacts, such as the head holder (as indicated in the circle) appear during the 3D reconstruction of the skull, which is not part of the brain and thus must be removed from further processing. In addition, we perform the projection in transverse section to produce the following figure (Figure 2.7) in binary image format:

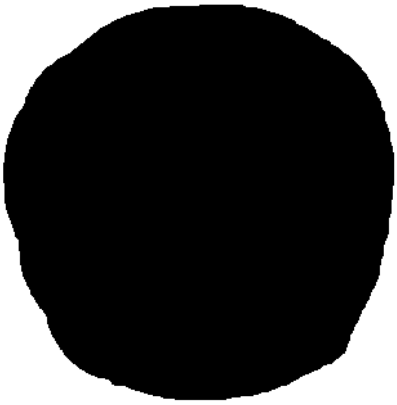

FIGURE 2.7: TRANSVERSE PROJECTION OF THE HEAD.

The rotation is done iteratively, from -5 (anticlockwise) to $+5$ (clockwise) degrees inclusively with the increment of 0.1 degree. The iteration involvs several intermediate steps:

(Initialization) Set angle $q := -5$

REPEAT

Step 2.1: Rotate the image with angle q to give $I_q(x, y)$.

Step 2.2: For each rotation, find the maximum inscribed rectangle to the transverse sectional images.

Step 2.3: For each rotation, flip the image obtained in Step 2.2 into half along the mid-sagittal plane to give $I'_q(x, y)$ and define error terms as the measure of the deviation between the left side and right side of the skull.

$$E(q) := I'_q(x, y) - I_q(x, y). \tag{2.1}$$

Update angle $q := q + 0.1$

UNTIL $q > 5$

Step 2.4: Among all angles $q \in \{-5, -4.9, \cdots, 4.9, 5\}$, find out the least error in Step 2.3, that is,

$$\{q \mid E(q) = \min_q E(q)\}. \tag{2.2}$$

The following figure demonstrates how to find the optimal orientation of the brain.

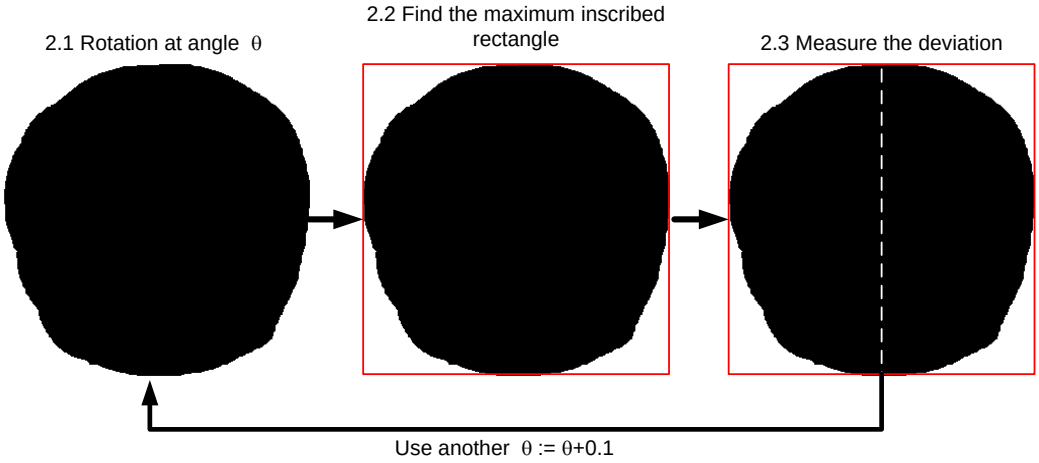

FIGURE 2.8: STEP 2 OF ALGORITHM 2.1.

The angle obtained in Step 2.4 may not be unique; therefore, we choose the angle with the least absolute value.

The next step is to find out the intracranial content of the brain. The intensity of the images is proportional to the attenuation of X-ray. By convention, water is defined as 0 Hounsfield Unit (HU), and air is –1000HU, the other tissue can be calibrated according to the pixel value of water, i.e.,

$$1000 \times \frac{m_x - m_w}{m_w}, \tag{2.3}$$

where m_x is the pixel value of tissue, and m_w is the pixel value of water. The skull has the higher attenuation value with CT numbers ranging from 80 to 1000 (Hounsfield Units). In most of the cases, the bony part of the skull can be removed from the images by global thresholding [23]. However, some regions such as calcification will be removed using global thresholding (as shown in the Figure 2.9) and other small external structures cannot be removed around the perimeter of the intracranial content.

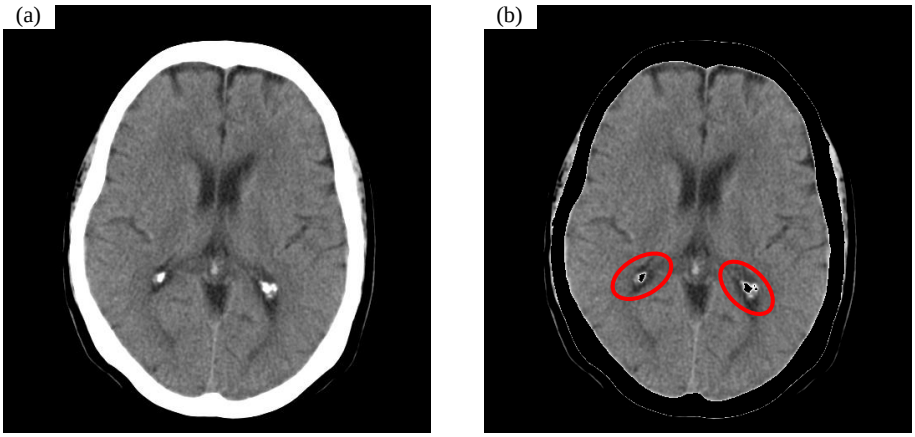

FIGURE 2.9: (a) ORIGINAL IMAGE; (b) BONE REMOVED USING GLOBAL THRESHOLDING, REGION OF CALCIFICATION (CIRCLE) ALSO REMOVED.

Therefore, we have proposed the following algorithm to preserve the calcification inside the brain

Algorithm 4.2 (Preserve the calcification):

1. Transform the CT image into binary image.
2. Remove the regions of calcification that have fewer than a certain number of square pixels, say 500 square pixels.
3. Remove the bone from the images with reference to the binary image.
4. Remove small external structures.

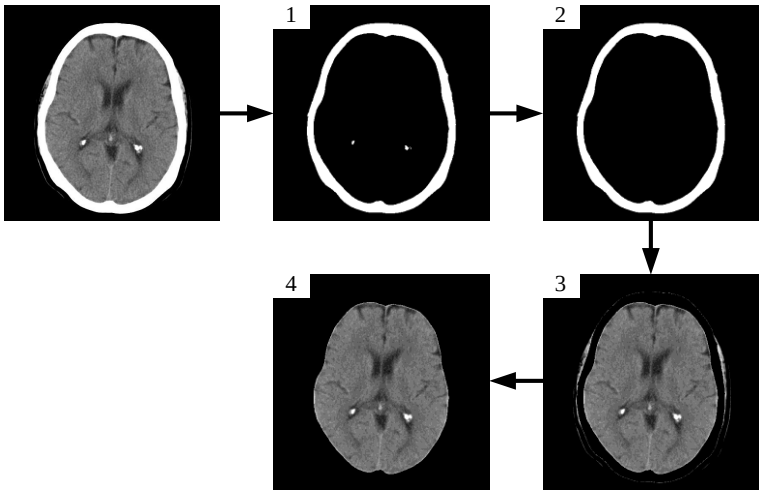

FIGURE 2.10: WORKFLOW OF ALGORITHM 2.2.

Different considerations are needed at different levels of the brain. For example, at the lower portion of the cranial cavity, segmentation of the eyeball is needed.

2.5.1 Features of Ischemic Stroke on CT

CT does not reveal much abnormal sign for the first 24 hours since the onset of ischemic stroke. The early detection solely relies on some important early adnormal signs, including loss of the insular ribbon (LIR) [24], attenuation of the lentiform nucleus (ALN) [25][26], hemispherical sulcus effacement (HSE), and the hyperdense middle cerebral artery sign (HMCAS), [27] [28]. Therefore, we need to incorporate these features into the CAD method so as to determine the early signs of ischemic stroke.

2.5.2 Proposed Algorithms

Proposition 2.1 (*Choice of appropriate section*): The largest section contains Anterior, Middle and Posterior Cerebral Artery (ACA, MCA and PCA) territory and basal ganglia.

This can be validated by using computer simulation.

After we extracted the appropriate section of CT, then we proposed an Adaptive Region of Interest (AROI) to find out the region with subtle change in the intensity at the Anterior, Middle and Posterior Cerebral Artery (ACA, MCA and PCA) territory, respectively, to detect an early infarct sign, which became conspicuous by our adaptive region of interest. The outline of Algorithm 2.3 is as follows:

Algorithm 2.3 (Adaptive region of interest):

1. Noise reduction by means of filter.
2. Generate Circular Adaptive Region of Interest.
3. Generate the binary mask according to Step 2.
4. Count the percentage of 0's over the boundary of binary mask in Step 3.
5. Find out the corresponding region from the other side.
6. Locate the region of possible abnormalities.
7. Detection is based on the parameters of images texture.

Step 1 is made to improve the quality of the images and increase the signal to noise ratio. Steps 2-4 will help us to find out the desired region of interest in a circular domain domain with various dimensions according to certain rules. Step 5 is used to find the corresponding region of interest from the contra-lateral sides. Steps 6-7 will help to locate the region of stroke using an optimization model and Artificial Neural Network (ANN).

A 3×3 averaging filter is applied to the original image, i.e.,

$$I * \frac{1}{9}\begin{bmatrix} 1 & 1 & 1 \\ 1 & 1 & 1 \\ 1 & 1 & 1 \end{bmatrix}, \tag{2.4}$$

where I is the sectional CT images and $*$ is the image convolution operator.

We apply the filter to the images so as to improve the image quality in terms of the peak signal to noise ratio (PSNR), which is given as.

$$PSNR = 10 \times \log_{10} \frac{\mathrm{MAX}_{\mathrm{I}}^2}{\mathrm{MSE}}, \tag{2.5}$$

where $\mathrm{MAX}_{\mathrm{I}}$ is the maximum possible pixel value of the image = 255 in the region and

$$MSE = \frac{1}{n^2}\sum_{i=0}^{n-1}\sum_{j=0}^{n-1}\left\|I(i,\ j) - K(i,\ j)\right\|^2 \tag{2.6}$$

is the mean square error of the image and $K(i,\ j)$ is the improved version of $I(i,\ j)$ using averaging filter. Typical values for the PSNR range between 30-50 dB, the higher the value of PSNR, the better the image quality.

The procedure will either process Steps 2-4 based on Circular domain.

Starting from the left side of the brain, a circular region of interest whose initial radius $r = 5$ pixels is assigned from the original image centered at (x_c, y_c). Therefore, the diameter of the initial circle is ($2r + 1$) pixels.

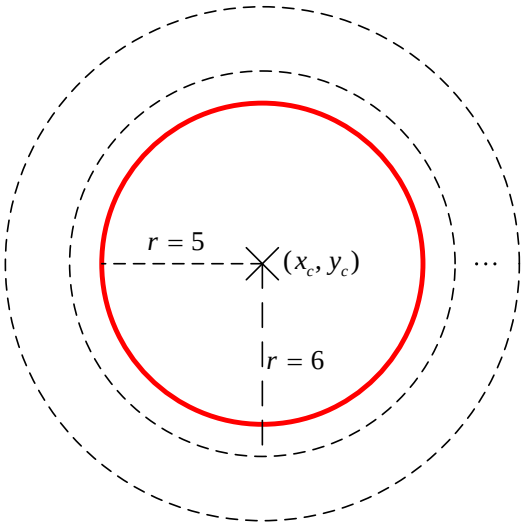

FIGURE 2.11: CIRCULAR ADAPTIVE REGION OF INTEREST.

The initial radius is 5 pixels because the size of the lacunar stroke is 15 mm in diameter, and the image resolution is about 3mm per pixel. Therefore, we choose $r = 5$ as our starting value.

For each point inside the circle of radius r, i.e., $||(i,\ j) - (x_c, y_c)|| \leq r$, we generate a binary mask based on the following criteria:

$$B_r(i,\ j) = \begin{cases} 0, & |\ I(i,\ j) - I(x_c, y_c)\ | > T, \\ 1, & |\ I(i,\ j) - I(x_c, y_c)\ | \leq T. \end{cases} \tag{2.7}$$

T distinguishes object region (mask value 1) and background region (mask value 0). A study by [29], suggested a value for $T = 3$ would be good enough to differentiate the boundary of the lentiform nucleus.

We calculate the percentage of 0's at the circumference from the binary mask, that is,

$$P_0 = \frac{\sum_{B_r(i,j)\cap(B_r(i,j)\cap B_{r-1}(i,j))^c=0} (1 - B_{r+1})}{\sum_{B_r(i,j)\cap(B_r(i,j)\cap B_{r-1}(i,j))^c=0,1} 1} \times 100\%, \tag{2.8}$$

where $(B_r(i,\ j) \cap B_{r-1}(i,\ j))^C$ refers to the boundary region of the binary mask.

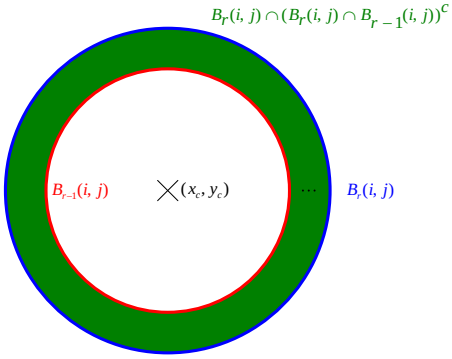

FIGURE 2.12: CIRCULAR BAND OF BOUNDARY IMAGE.

Stopping criteria of the adaptive region of interest: If $P_0 < 60\%$ in equation (4.8), then repeat again. The cut-off value of P_0 is chosen equal to 60% to indicate the adaptive region of interest is not homogeneous at all, i.e., a significant change in intensity from the center-point (x_c, y_c) to the boundary.

Step 6: Find out the corresponding region from another side

For each circle, we find out the corresponding circle on the right side of the brain, since the right side of the brain is almost the reflection from the left side of the brain if the case is normal. Therefore, we perform the reflection of the Adaptive circle on the right side of the brain. Then we can search the corresponding location by using Pearson's correlation coefficient R. It is widely used in the statistical analysis and medical image processing [30][31]. The Pearson's correlation coefficient can serve our purpose in the image registration, for monochrome digital images. The Pearson correlation coefficient is defined as

$$R = \frac{\sum_i (p_i - p_m)(q_i - q_m)}{\sqrt{\sum_i (p_i - p_m)^2} \sqrt{\sum_i (q_i - q_m)^2}}, \tag{2.9}$$

where p_i is the intensity of the i th pixel in the circle at the left side of the brain and q_i is the intensity of the i th pixel at the flipped right side of the brain, p_m and q_m are the mean intensity at the left side and flipped right side of the brain, respectively. The correlation coefficient has the value 1 if the two images are identical, 0 if they are not correlated.

Step 7: Locate the region of possible abnormalities

Within the circle, find out the corresponding region with least correlation.

Step 8: Detection is based on the parameters of image texture

Identify the region of genuine stroke according to the size of lesion, anatomical location, relationship between the surrounding structures, such as the midline shift of the brain, image intensity. The above parameters will be quantified by mathematical terms and will be discussed in the next section.

2.5.3 Factor Evaluation

Using Texture Analysis (TA) to study the images features has been used by many authors [32][33]. The Grey Level Co-occurrence Matrix (GLCM) is used to extract the information from an image. Given an image of size $m \times n$, parameterized by an offset $(\Delta x, \Delta y)$ the Co-occurrence matrix of size 8×8 is calculated as

$$C(i,j) = \sum_{p=1}^{m} \sum_{q=1}^{n} \begin{cases} 1, & \text{if } I(p,q) = i \text{ and } I(p+\Delta x, q+\Delta y) = j, \\ 0, & \text{otherwise.} \end{cases} \tag{2.10}$$

$C(i, j)$ will represent how often a pixel with the intensity (gray-level) value i occurs in a specific spatial relationship to a pixel with the value j. We can specify other spatial relationships between two pixels. The following figure (Figure 4.14) show how a 3×3 grayscale image I is transformed into the co-occurrence matrix C.

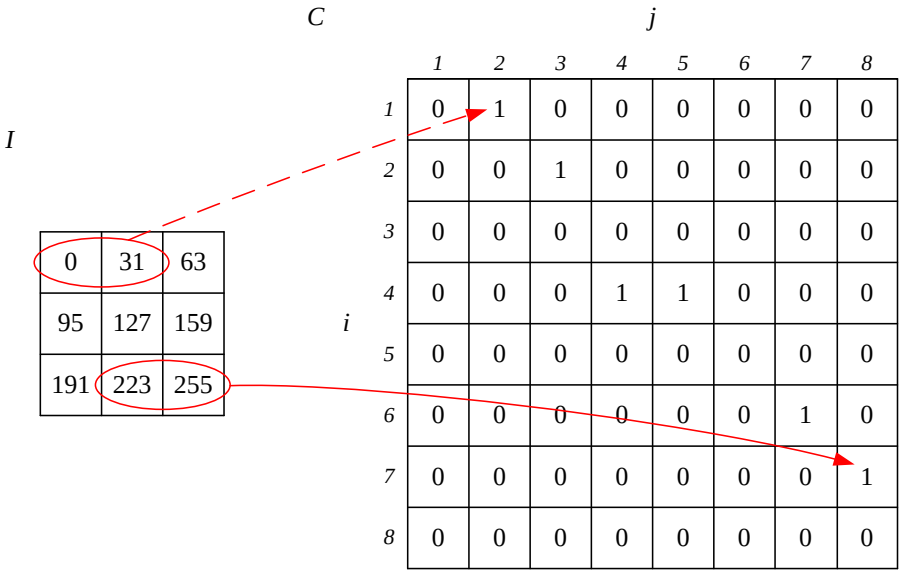

FIGURE 2.13: GENERATION OF CO-OCCURRENCE MATRIX. (AN INTENSITY IMAGE (0-255), IS SCALED TO 8 LEVELS, ELEMENT (1,2) IN THE GLCM HAS THE VALUE 1 BECAUSE THERE IS ONLY ONE INSTANCE IN THE INPUT IMAGE WHERE TWO HORIZONTALLY ADJACENT PIXELS HAVE THE LEVEL 1 AND LEVEL 2).

Based on the information of the co-occurrence matrix, we can apply the histogram statistics to produce the texture attributes [34]. The attributes can be derived from the co-occurrence matrix and they are denoted by A1-A8.

Energy: $$\sum_{i,j} C(i, j)^2 \quad \text{(A1)}$$

Entropy: $$-\sum_{i,j} C(i, j)\log C(i, j) \quad \text{(A2)}$$

Inverse difference moment: $$\sum_{i,j} \frac{1}{1+(i-j)^2} C(i, j) \quad \text{(A3)}$$

Inertia: $$\sum_{i,j} (i-j)^2 C(i, j) \quad \text{(A4)}$$

Shade: $$\sum_{i,j} (i+j-\mu_x-\mu_y)^3 C(i, j) \quad \text{(A5)}$$

Prominence: $$\sum_{i,j} (i+j-\mu_x-\mu_y)^4 C(i, j) \quad \text{(A6)}$$

Correlation: $$-\sum_{i,j} \frac{(i-\mu_x)+(j-\mu_y)}{\sqrt{(\sigma_x\sigma_y)}} C(i, j) \quad \text{(A7)}$$

Variance: $$\sum_{i,j} (i-\mu)^2 C(i, j), \quad \text{(A8)}$$

where μ_x, μ_y, σ_x and σ_y represents the mean and standard deviation of row or column sum, respectively, and μ represents the mean of the co-occurrence matrix.

Analysis of the parameters: The energy of a texture describes the uniformity of the texture. In a homogeneous image, the co-occurrence matrix has a fewer entries of large magnitude and the energy of an image is high when the image is homogeneous. The entropy measures the randomness of the element. For homogeneous image, the entropy should be low. The inverse difference moment, will give a higher value when the diagonal of C is high, while the inertia will give a larger value when the C has a higher value away from the diagonal. The inertia and the inverse difference moment are measures of the distribution of grey-scales in the image. Shade and prominence are the measures of skewness of C. The image is not symmetric when shade and prominence are high.

The above attributes will be calculated between the contra-lateral sides and then ordered into a row of vectors for further analysis, i.e.,

$$L_i = [A_1, A_2, A_3, A_4, A_5, A_6, A_7, A_8],\ i = 1, 2, \cdots, N, \tag{2.11}$$

$$R_i = [A_1, A_2, A_3, A_4, A_5, A_6, A_7, A_8],\ i = 1, 2, \cdots, N, \tag{2.12}$$

where L_i, R_i contain the image features of left side and right side of the brain respectively and N is the total number of images.

2.6 Consideration for Asymmetric Brain

Our methods solely rely on the comparison between the contralateral sides of the brain, and so may not work well for some of cases due to non-symmetry of the brain (Figure 2.14).

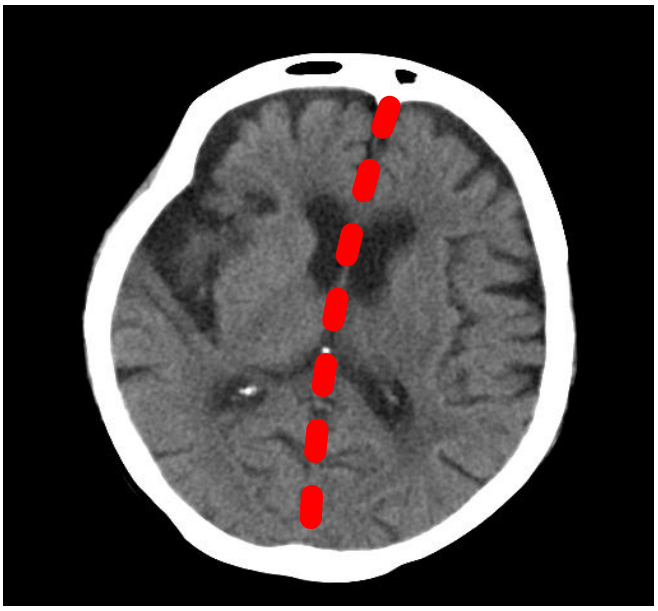

FIGURE 2.14: NON-SYMMETRIC CASE.

Therefore, tracing the anatomical midline (indicated by the dotted line) of the brain will be a good indicator to help comment on the degree of symmetry of the brain. In general, the anatomical midline is not easy to detect. We propose the following method for tracing the midline of the brain.

Algorithm 2.4 (Tracing midline of the brain):

Step 1: Read the image and preprocess to remove the image artifacts.

Step 2: For each row of the image, convert the image into 1D vector.

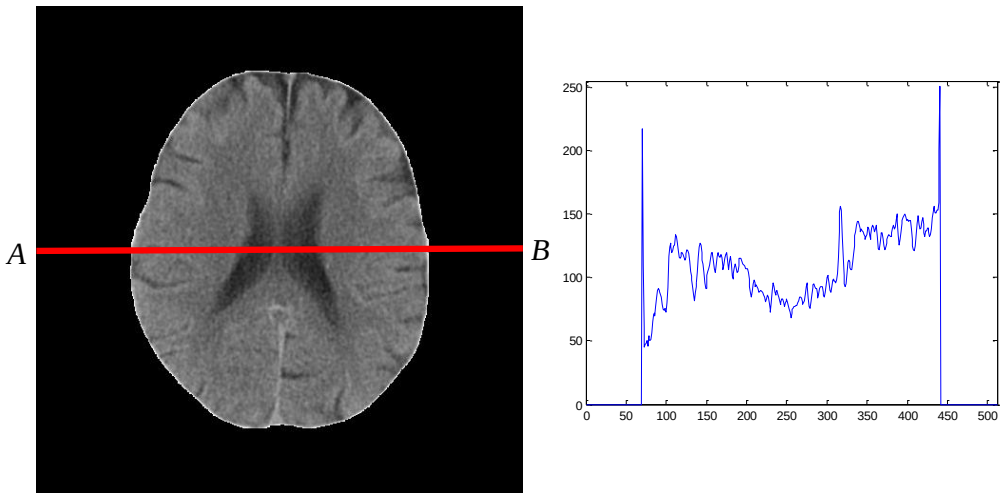

FIGURE 2.15: INTENSITY DISTRIBUTION OF A SINGLE ROW ALONG AB.

Step 3: For each row of the image, find out the center-point by the method of cross-correlation between the original 1D vector and the flipped 1D vector. The center-point will be the location with the largest value of cross-correlation.

Step 4: Joining all the center-points of each row will give the trace of the midline, given by

$$i = f(x_i),\ i = 1, 2, \ldots, m, \tag{2.13}$$

where m is the number of rows of the image.

For a normal brain, the midline will occur at half of the CT image. If the midline obtained in step 4 is far from the midline, then

$$\left| x_i - \frac{n}{2} \right| > \sigma_x, \tag{2.14}$$

where n is the number of columns of the image and σ_x is the standard deviation of all the x-coordinates of the center-point. Additional rules need to be applied to check the normality of the brain. We now differentiate the L/R of the brain based on the anatomical midline. The following attributes should be realized at the contra-lateral sides in the detection of stroke:

- Loss of insular ribbon
- Loss of gray-white interface
- Loss of sulci
- Acute hypo density
- Mass effect
- Dense MCA sign

In case of asymmetry, step 6 of Algorithm 2.3 should be made with reference to the anatomical midline in Algorithm 2.4.

III. CONCLUSION AND FUTURE WORKS

In this paper a CAD scheme using Adaptive Region of interest and Ischemic Stroke has proposed. In order to help the Radiologists achieve a higher level of sensitivity and specificity, evaluation of a CAD scheme using Receiver Operating Characteristic (ROC) analysis will be carried out clinically.

ACKNOWLEDGEMENTS

The authors would like to thank Professor James Caldwell, Honorary Professor, The Open University of Hong Kong for his great encouragement and for his efforts in the copy editing of this paper.

REFERENCES

[1] Adams M.A., Dubnick M., et al. (1992). Sequence identification of 2,375 human brain genes. Nature. 355:632-634.

[2] Centers for Disease Control and Prevention (CDC). (2007). Prehospital and hospital delays after stroke onset—United States, 2005-2006. MMWR Morb Mortal Wkly Rep. 56(19):474-8.

[3] Hui, A.C.F., & Wong, K.S. (2002). Update in prevention of ischaemic stroke. The Hong Kong Practitioner. 24:344-353.

[4] Muir K.W. (2001). Magnesium for neuroprotection in ischaemic stroke: rationale for use and evidence of effectiveness, CNS Drugs. 15:921–930.

[5] Jennett B. & Teasdale G. (1981). Management of head injuries. 2nd ed. Philadelphia: F.A. Davis, 1981.

[6] U.S. Department of Health and Human Services. Public Health Service, Agency for Health Care Policy and Research. (1995). Post-Stroke Rehabilitation. Clinical Practice Guidelines. Rockville, MD.

[7] Kucinski T., Vaterlein O., et al. (2002). Correlation of apparent diffusion coefficient and computed tomography density in acute ischemic stroke, Stroke. **33**:1786-1791.

[8] Weinstein M.C., & Stason W.B. (1977). Foundations of cost-effectiveness analysis for health and medical practices. N Engl J Med. 296:716-721.

[9] Adams, H., Adams R., et al. (2005). Guidelines for the early management of patients with ischemic stroke: 2005 guidelines update a scientific statement from the Stroke Council of the American Heart Association/American Stroke Association. Stroke. 36(4):916-23.

[10] Chalela J.A., Kidwell C.S., et al. (2007). Magnetic resonance imaging and computed tomography in emergency assessment of patients with suspected acute stroke: a prospective comparison. Lancet. 369(9558):293-8.

[11] Sitburana O. & Ondo W.G. (2006). Tetrabenazine for hypoglycemic induced hemichorea-hemiballismus. Mov Disorders. 21:2023-5.

[12] Aronovich B.D., Reider-Groswasser II., et al. (2004). Early CT changes and outcome of ischemic stroke. Eur J Neurol.11:63-65.

[13] Sarkarti D. & Reisdorff E.J. (2002). Emergent CT evaluation of stroke. Emerg Med Clin North Am. 20:553-81.

[14] Schriger D.L., Kalafut M., et al. (1998) Cranial computed tomography interpretation in acute stroke: physician accuracy in determining eligibility for thrombolytic therapy. JAMA. 279:1293-1297.

[15] Taylor P., Champness J., et al. (2005). Impact of computer-aided detection prompts on the sensitivity and specificity of screening mammography. Health Technology Assessment. 9(6):1-70.

[16] Fenton J.J., Taplin S.H., et al. (2007). Influence of computer-aided detection on performance of screening mammography. N Engl J Med. 14:1399-409.

[17] Pereira R.R., Azevedo Marques P.M., et al. (2007). Usefulness of texture analysis for computerized classification of breast lesions on mammograms. J of Digital Imaging. 20:248-255.

[18] Wu N., Gamsu G., et al. (2006). Detection of small pulmonary nodules using direct digital radiography and picture archiving and communication systems. J Thorac Imaging. 21(1):27-31.

[19] Li F., Engelmann R., Metz C.E., Doi K., et al. (2008). Lung cancers missed on chest radiographs: Results obtained with commercial computer-aided detection program. Radiology. 246: 273-280

[20] Unsold R., DeGrott J., et al. (1980). Images of the optic nerve. Anatomic-CT correlation. AJNR. 1:317-323.

[21] Silverman C.S. & Mancuso A.A. (1998). Periantral soft-tissue intiltration and its relevance to the early detection of invasive fungal sinusitis: CT and MR findings. AJNR. 19:321-325.

[22] Doi K. (2007). Computer-aided diagnosis in medical imaging: Historical review, current status and future potential. Computerized Medical Imaging and Graphics. 31(4-5):198-211

[23] Chan T. (2007). Computer aided detection of small acute intracranial hemorrhage on computer tomography of brain, Computerized Medical Imaging and Graphics. 07(4-5):285-298.

[24] Truwit C.L., Barkovich A.J., et al. (1990). Loss of the insular ribbon: another sign of CT infarction. Radiology. 176:801-806.

[25] Tomura N., Uemura K., et al. (1998). Early CT finding in cerebral infarction: obscuration of the lentiform nucleus. Radiology. 168:463-467.

[26] Bozzao L., Bastianello S., et al. (1989). Correlation of angiographic and sequential CT findings in patients with evolving cerebral infarction. AJNR Am J Neuroradiol. 10:1215–1222.

[27] Gács G., Fox A.J., et al. (1983). CT visualization of intracranial arterial thromboembolism. Stroke. 14:756-762.

[28] Pressman B.D., Tourje E.J., et al. (1987). An early CT sign of ischemic infarction: increased density in a cerebral artery. AJNR Am J Neuroradiol. 8:645–648.

[29] Lee Y., Takahashi N., et al. (2006). Detectability improvement of early sign of acute stroke on brain CT images using an adaptive partial smoothing filter, Proc. of SPIE Medical Imaging 2006. 6144:2138-2145.

[30] Fons B., Harm M., et al. (1998). The use of a transverse CT image for the estimation of the dose given to the rectum in intracavitary brachytherapy for carcinoma of the cervix. Radiotherapy and Oncology. 47(1):85-90.

[31] Cheng L.L., Chang I.W., et al. (1998). Correlation of High-Resolution Magic Angle Spinning Proton Magnetic Resonance Spectroscopy with Histopathology of Intact Human Brain Tumor Specimens. *Cancer Research.* 58:1825-1832.

[32] Cheng H.D., Cai X.P., et al. (2003). Computer-aided detection and classification of microcalcifications in mammograms: a survey, Pattern Recognition. 36:2967-2991.

[33] Ferro J.M., Canhao P., et al. (2004). Prognosis of cerebral vein and dural sinus thrombosis (ISCVT). Stroke. 35:664-70.

[34] Haralick R.M., Shanmugam K., et al. (1973). Textural Features for Image Classification. IEEE Transactions on Systems, Man, and Cybernetics. 3(6):610–621.